Available online at www.sciencedirect.com
SCIENCE DIRECT®
Biochemical and Biophysical Research Communications 327 (2005) 361–370
BBRC
www.elsevier.com/locate/ybbrc

Peptide antibiotic and actin-binding protein as mixed-type inhibitors of *Clostridium difficile* CDT toxin activities

Dario Cruz Angeles, Keang Peng Song*

Microbial Pathogenesis Laboratory, Department of Microbiology, Faculty of Medicine, National University of Singapore, Singapore 117597, Singapore

Received 18 November 2004
Available online 18 December 2004

Abstract

CDT from *Clostridium difficile* is an ADP-ribosyltransferase that causes rapid actin disaggregation and cell death. For efficient catalysis, CDT required specific divalent cations and binding by NAD which can be substituted by ATP but not ADP. Increasing isolation of CDT-producing strains prompted our search for antagonists like the anti-*C. difficile* agents bacitracin and vancomycin which were effective CDT inhibitors. Other CDT transferase and glycohydrolase inhibitors with consistently low IC_{50} values were heterocyclic peptide antibiotics containing modified amino acids such as polymyxin B and β-lactam cephalosporins. The strongest inhibitors were actin-binding proteins which possess extensive interfaces with G-actin, adjoining the CDT–ADP-ribose$^+$ acceptor site and nucleotide cleft. Analysis of the extent and mode of inhibition and actin interaction sites provided fresh evidences on the designation of actin interface domains with actin-binding proteins. Our results uphold ADP-ribosylation as an innate physiologic process in cellular cytoskeletal reorganization regulated by endogenous metabolites.

Keywords: *Clostridium difficile*; ADP-ribosyltransferase; NAD glycohydrolase; Enzyme inhibition; Actin-binding protein

Aside from ATP phosphorylation and GTP-protein binding, ADP-ribosylation is a post-translational, protein-modification process involved in many cellular functions [1,2]. Eukaryotes produce nuclear poly(ADP-ribosyl) synthetase which mediates substrate linkage of several ADP-ribose moieties and mono (ADP-ribosyl) transferase which is likewise produced by prokaryotes. The catalytic process involves *N*-glycosidic bond hydrolysis of NAD^+ resulting in the release of nicotinamide and attachment of adenosine-diphosphoribose group to an acceptor protein [3]. A variety of acceptor molecules have been identified such as histones, enzymes, and regulatory and structural proteins [2,4,5].

Several bacterial ADP-ribosyltransferases (ADPRT) induce disease by modifying essential biologic effectors that undermine host homeostasis. Among these are cholera toxin which impedes cell signaling through ADP-ribosylation of heterotrimeric G-protein coupled receptors and diphtheria toxin which modifies elongation factor 2 disrupting protein synthesis [6,7]. *Clostridium botulinum* exoenzyme C3 monoglucosylates Rho GTPases [7] whereas *Pseudomonas aeruginosa* ExoS terminal domains affect various substrates [8].

Clostridium difficile CDT belongs to a subfamily of binary actin-ribosylating toxins which includes *C. botulinum* C2, *Clostridium perfringens* iota, and the *Clostridium spiriforme* toxin [9,10]. The genes *cdtA* and *cdtB* code for the unlinked enzyme (CDTa) and binding/translocation components (CDTb), respectively, which must be trypsin-activated to function [11]. Reminiscent of C2 toxin action [12], CDTa ADP-ribosylates monomeric actin, inactivating its ATPase and nucleating activities which cause cytoskeletal collapse and cytolysis. The bulky ADP-ribose group is attached to arginine-177 of actin subdomain III forming bulk hindrance that

* Corresponding author. Fax: +65 67766872.
E-mail address: micskp@nus.edu.sg (K.P. Song).

0006-291X/$ - see front matter © 2004 Elsevier Inc. All rights reserved.
doi:10.1016/j.bbrc.2004.11.167

prevents actin polymerization [13]. The acceptor amino acid is embedded in the filamentous actin form, thus explaining F-actin role as a poor CDT substrate.

The ubiquity of actin and high equimolar concentration of G- and F-actin forms reflect its diverse physiologic roles that must be protected against modifying agents through the development of effective inhibitors. Indeed, there has been an increase in the isolation of *cdt*-encoding pathogenic *C. difficile*, an organism implicated in mammalian enterotoxemia, antibiotic-associated diarrhea, and colitis [14–16]. Previous studies have focused largely on compounds against eukaryotic poly(ADP-ribosyl) synthetases whose inhibitory actions were found to be highly specific [17,18]. In fact, differences in inhibitory capability yielded a broad range of ordered efficacy. While novobiocin, vitamin K_1, and vitamin K_3 were reported to be most potent for eukaryotic mono (ADP-ribosyl) transferase from hen heterophil, preventive efficacy of the vitamin derivative nicotinamide has differed depending on ADPRT source [17,19]. Here we report in vitro effects of several groups of natural and synthetic compounds such as metal ions, nucleotides, antimicrobials, vitamins, and actin-binding proteins (ABPs) on bacterial mono ADPRT activities. The most potent inhibitors were α-actinin and striated muscle thin filament constituents, antagonistic to specific CDT actions.

Materials and methods

Materials. Clostridium difficile strains were obtained from Culture Collection University of Göteborg (CCUG) and Virginia Polytechnic Institute (VPI). Colorectal carcinoma HCT 116 cells were from the American Type Culture Collection. [*adenylate*-^{32}P]NAD, [*nicotinamide*-^{3}H]NAD, and [6-^{3}H]thymidine were from Amersham Biosciences and DNase I-Oregon green 488 was from Molecular Probes (Eugene, OR). Toxin A expression was measured using ELISA (TechLab, VA). Phalloidin–tetramethylrhodamine isothiocyanate (TRITC), muscle actin, trypsin, trypsin inhibitor, and analytical grade compounds were from Sigma (St. Louis, MO). Chemicals were dissolved in dimethyl sulfoxide (DMSO) as 1 mM working solution except for the actin-binding proteins.

Derivation and purification of CDT. C. difficile virulence gene fragment insert from genome-subtracted library clone GS80 (GenBank Accession Nos. CC927338–CC927348) was traced to *cdtB* of CD196 [11]. Primer pairs cda-F1/R1 (5′-TTGCAATACTACTTACAAGG CTTC-3′/5′-TCATATTCAGGGGAAGTAAGAGTTA-3′) and cdb-F1/R1 (5′-ACTCCCAAACAATGGATTAATGGG-3′/5′-TTGACA TTACTCCATGTACTAGGG-3′) were designed for screening *C. difficile* strains and cloning *cdt orfs* from CCUG20309 into pCR2.1. Identical primers flanked with restriction sites were used for directional cloning in expression vector pQE-30. Transformants SK1214 (pDA577), SK1215 (pDA578), and SK1216 (pDA576) with respective *cdtA*, *cdtB*, and *cdtA*/*B* constructs fused N-terminally to 6× Histidine tag under T7 promoter control were expressed. Recombinant CDTs were purified using Ni–NTA affinity chromatography as described (Qiagen). Eluate fractions (1 ml) were analyzed in 10% SDS–PAGE, then desalted and concentrated by ultrafiltration using YM-30 and YM-50 MW membranes (Millipore, MA). Cytoplasmic extract from SK1203 (M15 with pQE-30) was also purified as assay control. CDT proteins were activated in 200 μg/ml trypsin–Tris buffer for 20 min at 37 °C followed by 300 μg/ml trypsin inhibitor for 30 min.

Thymidine assimilation. Incorporation of DNA precursor [^{3}H]thymidine upon CDT treatment was compared with SK1203-treated control. HCT 116 monolayer maintained in McCoy's 5A (Sigma, MO) and routinely passaged at 1:8 subcultivation ratio was reseeded into 25 cm^2 tissue culture flask with 5×10^4 cells and grown for 20 h to partial confluency. Medium was replaced with that containing [^{3}H]thymidine at 20 mCi/mmol with 200 ng/ml CDTb for 15 min followed by 100 ng/ml CDTa or SK1203 protein or individual CDT components. At designated timepoints, cells were lysed in 0.5% Triton X-100 in 40 mM Tris–HCl, pH 7.5. After 10 min centrifugation at 13,000 rpm, supernate aliquot was mixed with scintillant cocktail (1:10) and radioactivity was measured using MicroBeta liquid scintillation counter (Perkin–Elmer, MA). Experiments were performed in four trials with batch counts detected thrice. Data values in counts per minute were corrected by subtraction of background counts from control.

Confocal microscopy. HCT 116 monolayer was reseeded onto six-well plates with coverslips at 5×10^5 cells/well, and then incubated in 200 μl medium containing 200 ng/ml CDTb for 15 min followed by 100 ng/ml SK1203 or CDTa with or without 50 μg inhibitor preincubation. Plates were incubated for 8 h before processing and staining as recommended (Molecular Probes). Fluorescent conjugates DNaseI-Oregon green (ex., 496; emm. 524 nm) and phalloidin–TRITC (ex. 385; emm. 470 nm) were used as tandem stains. Cells were mounted on 60% glycerol–PBS, sealed with nail polish, and observed at 10% argon ion laser power (488) nm for Oregon green and 10% helium neon laser (543 nm) for TRITC. Percent cytotoxicity counts were calculated from eight fields of 400× magnified micrograph images per timepoint.

ADP-ribosylation assay (ARTase). The level of CDT-mediated attachment of ADP-ribose to actin was quantified according to methods described [20]. The 40 μl total assay mixture contained 100 ng/ml CDTa, [adenylate-^{32}P]NAD at 25 mCi/mmol (0.5 μM), 40 μg/ml HCT 116 lysate protein or 3 μg muscle actin, 1 mM DTT, 40 μM ATP, 50 μM $CaCl_2$, and 50 μM $MgCl_2$ in 40 mM Tris–HCl, pH 7.5. Inhibition assay mixture containing CDTa and actin was routinely preincubated with inhibitor compound at 50, 100, 200, and 400 μM concentrations for 20 min prior to addition of labeled NAD and further incubation for 1 h at 37 °C. Thereafter, 2× SDS–PAGE loading buffer was added to the reaction mixture before separation in 12% SDS–PAGE. The gel was dried, exposed to general-purpose phosphor storage screen, and scanned on Typhoon phosphorimager (Amersham). Bands were measured in pixel unit corrected for background signals from buffer-treated controls and standardized with respect to corrected mean positive control values. Experiments were conducted in triplicate and images were analyzed using the Total lab software.

NAD glycohydrolase assay (NADse). The level of NAD hydrolysis by CDTa was determined as described [21]. The 50 μl reaction mixture contained 100 ng/ml CDTa, [*nicotinamide*-^{3}H]NAD at 30 mCi/mmol, 10 mM DTT, 20 μg BSA, and specified inhibitor concentration in 40 mM Tris–HCl (pH 7.5) incubated for 1 h at 37 °C. Free nicotinamide was extracted by the addition of 250 μl water-saturated ethyl acetate, 300 μl of which was mixed with 1.8 ml scintillant cocktail and the amount of radiolabeled nicotinamide was determined using liquid scintillation counting. Quadruplicate assays were performed and measurements were corrected by subtraction of background values from non-specifically hydrolyzed NAD.

Photoaffinity labeling. NAD binding to actin by photo-crosslinking was determined. For saturation studies, the 40 μl reaction mixture contained 1 μg actin incubated for 5 min with increasing concentrations of [*adenylate*-^{32}P]NAD in 40 mM Tris–HCl prior to UV irradiation for 10 min at 5 cm distance, 254-nm, and 60 W/cm^2 intensity (Ultra-Lum, CA). For competition studies, [^{32}P]NAD at 50 mCi/mmol was irradiated in the presence of 2 μg actin or 300 ng/ml CDTa which was preincubated for 5 min with increasing ATP or NAD. For protection studies 100 ng/ml CDTa was preincubated with specified

compound (inhibitor/inducer) concentrations. Proteins were resolved in 12% SDS–PAGE and analyzed by phosphorimaging.

Results

Characterization of CDT and nucleotide binding

Functionality of purified CDT was assessed before interaction with potential inhibitors. Initially, pathogenicity of strains (DNA sources) for subtractive hybridization and cloning was ascertained through toxin A expression. As in pathogen CCUG19126 (0.589), CCUG20309 (0.446) produced toxin A but not non-pathogenic VPI11186 (0.036, $p < 0.01$). The *cdt* amplicons of 0.9 (*cdta*), 1.8 (*cdtb*), and 3.2 (*cdta*/*cdtb*) kb sizes were generated only from CCUG20309 (data not shown). These indicate the presence of CCUG20309-encoded virulence genes from the pathogenicity and *cdt* loci. pDA576 construct expressed proteins of ~53 (CDTa) and 99 kDa (CDTb) sizes (Fig. 1A), matching molecular masses from CD196 [11]. To test its cytotoxicity, temporal effects on thymidine incorporation by human colon cells in vitro were measured as indicator of growth. As shown in Fig. 1B, there was declining growth trend among cells treated with binary CDT relative to SK1203, CDTa or CDTb alone in all timepoints ($p = 3–6 \times 10^{-3}$, $p < 0.01$). Although single component treatments were not significant, there were consistently lower mean counts for CDTb suggesting its influence on cytolysis possibly through membrane perturbation, aside from its role in translocation.

On testing direct CDTa action on actin, ADP-ribosylation proceeded in a time-dependent manner having peaked at 1 h mark (197.32) (Fig. 1C). Proportional rise in CDTa dosage and actin labeling (Fig. 1D) supported substrate specificity of CDT action. NAD binding to actin was then determined via UV cross-linking. Photoinsertion into actin was proportional to [^{32}P]NAD concentration with saturation effects observed at 46 μM (Fig. 1E). Competition for binding by increasing unlabeled parent nucleotide resulted in corresponding decrease in radiolabeling (Fig. 1F) with half-maximal prevention obtained at 42.7 μM. These demonstrate specificity of [^{32}P]NAD interaction with actin nucleotide binding site. Since attachment of NAD to CDT catalytic site was requisite in ADP-ribosylation, we next compared the prevention of [^{32}P]NAD photoinsertion into CDT by increasing NAD and ATP. Both nucleotides prevented photoinsertion with ATP causing 16% while

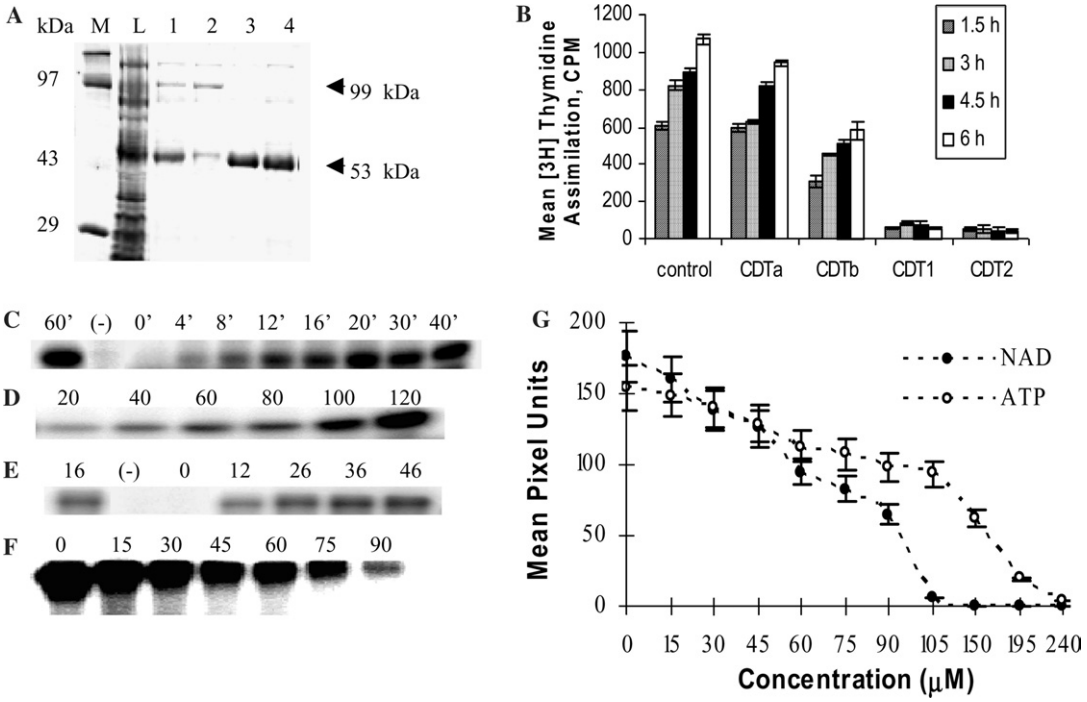

Fig. 1. Characterization of recombinant CDT. (A) Purified cytoplasmic extract and recombinant protein profiles in 10% SDS–PAGE. Lanes 1–4, buffer eluates D1, D2, E1, and E2, respectively, from SK1216 lysate. M, protein ladder; L, crude lysate. (B) Time-course analysis of [^{3}H]thymidine assimilation by HCT 116. Control is treated with pooled SK1203 eluate; CDTa at 200 ng/ml concentration; CDTb at 400 ng/ml; and CDT1 and CDT2 were sequentially treated with 400 ng/ml CDTb followed by 100 and 200 ng/ml CDTa, respectively. Biochemical functions of CDT and actin. (C) Time-course analysis of actin-directed ADP-ribosylation arrested at indicated times. Purified SK1203 (0.5 μg) was substituted for CDTa in the (−) lane. (D) ADP-ribosylation with increasing CDTa in increasing concentrations (ng/ml). (E) Saturation of actin nucleotide binding site by photolabeling with increasing [^{32}P]NAD concentrations (mCi/mmol). No actin was added for the (−) lane. (F) Prevention of [^{32}P]NAD photolabeling of actin with increasing NAD concentrations (μM). (G) Comparative prevention of [^{32}P]NAD photoinsertion into CDT by NAD and ATP at increasing concentrations (μM).

NAD caused 29% prevention (Fig. 1G), indicating higher NAD affinity to CDT nucleotide binding site. For control reactions, non-irradiated reaction mixtures and those with CDT or actin alone showed no detectable band indicating the absence of autologous phosphorylation and endogenous or contaminant radiolabels.

Divalent metal ions enhanced CDT-NAD binding

We then quantified the effects of ionic compounds on NAD photolabeling of CDT to detect cofactors which could hasten or inhibit biochemical reactions. Relative to $MgCl_2$ (maximal activity) with mean pixel value of 62, $ZnCl_2$ at 112, and $MnCl_2$ at 79 U enhanced photoinsertion by 81% and 27%, respectively, while Ca^{2+} and other monovalent ions weakened reactions by 2–7% indicating inability to substitute for Mg^{2+} (Figs. 2A–C). This was reflected in phosphorimages showing distinctly stronger intensities for Mn^{2+} and Zn^{2+} ions particularly at 100 μM and still evident at higher concentration. When chelators were added, differential reduction in labeling was observed (Fig. 2D), implicating the influence of metal ions in nucleotide binding. At 50 μM concentrations, the effect of $ZnCl_2$ was lowered upon EGTA (62%), EDTA (43%), and calmodulin (37%) preincubation. $MgCl_2$ and $MnCl_2$ effects were diminished except by calmodulin which enhanced photoinsertion by 14–27%. EDTA lowered Zn^{2+}, Mn^{2+}, and Mg^{2+} effects by 43%, 38%, and 34%, respectively. EGTA caused 49% reduction on Mg^{2+} and only 26% on Mn^{2+} effects. Such divergent influence signifies a pattern of hierarchy for functional specificity of ionic species on NAD attachment to CDT. Overall, Zn^{2+} and Mn^{2+} appeared to have fulfilled the metal-ion requirement more efficiently than Mg^{2+}.

Effects of various compounds on CDT activities

Several groups of compounds proved inhibitory to CDT actions (Table 1). The more potent among them were ATP and nitrogenous compounds. Consistent with its direct competition with the labeled counterpart (Figs. 1F and G), NAD expectedly posted a high significant reduction of 36% and 58% in ARTase and NADse activities, respectively ($p < 0.01$). This was reflected as decrease in actin radiolabeling (Fig. 2G) and free nicotinamide that corresponded to higher percentage inhibition of transferase and glycohydrolase activities (Table 1). Similar trends were observed on assay results performed at 50, 200, and 400 μM inhibitor concentrations (data not shown).

ATP caused weaker ARTase and NADse inhibition than NAD, while other nucleotides including ADP ($p = 0.39$) did not inhibit (Table 1) (Fig. 2G), except for AMP which lowered ARTse but not NADse reactions implicating its effect on actin Arg177–ADP-ribose

Fig. 2. Representative phosphorimages showing the effects of various compounds on CDT actions. Effects of cations and chelators on [^{32}P]NAD photoinsertion into CDT. (A–C) CDTa incubated with $CaCl_2$, $CsCl_2$, $RbCl_2$, $MnCl_2$, $MgCl_2$, and $ZnCl_2$ (lanes 1–6, respectively) at indicated concentrations. (D) CDT incubated with 100 μM $MnCl_2$, $MgCl_2$, and $ZnCl_2$ (lanes 1–3, 4–6, and 7–9, respectively) after preincubation with no chelator, 50 μM EDTA, and EGTA (lanes 1, 4, 7; 2, 5, 8; and 3, 6, 9, respectively). Effects of chemical compounds on ADP-ribosylation. (E) Preincubated with amoxycillin to cyclosporin A (lanes 1–11, respectively); (F) preincubated with erythromycin to thymine (lanes 12–26, respectively); and (G) preincubated with thymidine to nicotinic acid (lanes 27–40, respectively). Note that numerical assignment for each lane corresponds to a compound of the same numerical designation in Table 1. C1–C3, control lanes containing no inhibitor incubated with DMSO, without DMSO, and with SK1203 in DMSO, respectively. M, protein ladder. Effects of actin-binding proteins on ADP-ribosylation. (H) Preincubated with no inhibitor (lane 1), with 6 μg (lanes 2–5) and 12 μg (lanes 6–9) of α-actinin, myosin, tropomyosin, and troponin (lanes 2, 3, 4, 5 and 6, 7, 8, 9, respectively). (I) Photoaffinity labeling of actin with no inhibitor (lane 1), no actin (lane 2), and with 1 μg α-actinin, myosin, and tropomyosin (lanes 3, 4, and 5, respectively). Asterisk represents consistent inhibition in all three trials at varied concentrations (50, 100, 200, and 400 μM). Compound concentrations are indicated at the end of each lane series.

interaction rather than CDT-NAD. Contrastingly, nitrogenous bases particularly guanine showed prevention of NAD glycohydrolysis (Table 1). ADP, GTP, and UTP were not as preventive at concentrations up to 500 μM. Direct ATP competition for nucleotide binding sites in CDT or actin seems probable as inhibitory effects were evident in all biochemical assays performed. In general however, nucleotide prevention may involve metal ion chelation.

Of the antimicrobials tested, polymyxin B (PMB), penicillin G, and bacitracin prevented both ARTase and NADse activities (Table 1, Fig. 2). In decreasing

Table 1
Effects of various compounds on CDT enzymatic functions

Compound	Chemical nature	Molecular weight (kDa)	Transferase activity[a]		Glycohydrolase activity[a]	
			Mean % inhibition[b]	IC_{50} (μM)	Mean % inhibition[c]	IC_{50} (μM)
Amoxycillin	β-Lactam	365.4	0	n	12	833
Ampicillin	β-Lactam	349.4	−6	n	11	909
Bacitracin	Cyclic heptapeptide	1422.69	11	455	37	270
Cefotaxime	β-Lactam	477.45	8	625	38	263
Cefuroxime	β-Lactam	446.37	8	625	16	625
Cephradine	β-Lactam	349.4	6	833	38	263
Chloramphenicol	Nitrophenyl propanediol	323.13	2	2500	−12	n
Clindamycin	Lincosamide	424.93	−10	n	−19	n
Cloxacillin	β-Lactam	475.9	14	357	−25	n
Cycloheximide	Organophosphorus	281.3	8	625	17	588
Cyclosporin A	Cyclic oligopeptide	1202.64	6	833	35	286
Erythromycin	Macrolide	733.93	0	n	−2	n
Kanamycin	Aminoglycoside	483.93	0	n	18	556
Methicillin	β-Lactam	379.41	−1	n	−6	n
Nalidixic acid	Quinolone	232.24	−3	n	13	769
Nystatin	Polyene	926.13	−18	n	3	n
Penicillin G	β-Lactam	333.5	12	417	28	357
Polymyxin B	Basic cyclic decapeptide	1188	21	238	45	222
Streptomycin	Aminoglycoside	581.58	1	5000	11	909
Tetracycline	Tetracycline	443.44	0	n	6	1802
Trimethoprim	Sulfonamide	290.32	5	1000	5	2165
Vancomycin	Glycopeptide	1413	17	294	6	1686
Adenine	Nitrogenous base	135.13	3	1667	16	625
Guanine	Nitrogenous base	151.13	18	278	47	211
Cytosine	Nitrogenous base	111	5	1000	16	625
Thymine	Nitrogenous base	126	1	5000	15	646
Thymidine	Nucleoside	242.2	−12	n	16	608
Uracil	Nitrogenous base	112	−17	n	24	417
ATP	Nucleotide	507.18	21	238	34	294
ADP	Nucleotide	427.2	4	1250	1	n
AMP	Nucleotide	347.22	20	250	−8	n
GTP	Nucleotide	523.18	−8	n	2	n
UTP	Nucleotide	468.14	−3	n	−5	n
NAD	Nucleotide	663.43	36	139	58	172
Ascorbic acid	Theoascorbic acid	176.12	−5	n	23	435
Menadione (Vit K_3)	Methyl naphthoquinone	172.18	19	263	35	286
Pantothenic acid	Dimethyl oxobutyl alanine	219.24	−3	n	26	385
Thiamin	Aneurine	300.82	1	5000	41	245
Riboflavin	Flavin adenine dinucleotide	376.36	1	5000	28	357
Nicotinamide	Amide form of VitB3	122.13	12	417	16	625
α-Actinin	Actin crosslinker	100	64	78	42	236
Myosin	Actin binding	500	35	143	26	391
Tropomyosin	Myosin blocker	36/42	26	192	23	440
Troponin	Tropomyosin binding	38/24/18	−13	n	3	2961

n, non-inhibitory or low inhibition. Data interpretation: $IC_{50} < 400$, inhibition; 400–500, intermediate inhibition; >500, non-inhibition (ARTase); $IC_{50} < 300$, inhibition; 300–400, intermediate inhibition; and >400, non-inhibition (NADse).

[a] Assay mixture at 2% final DMSO concentration with 3 μg muscle actin.

[b] Calculated from mean values with reference to control (maximal activity, no inhibitor) from assay trials performed at least three times at 10 μg ABP concentration and 100 μM for all the other inhibitors.

[c] Calculated from mean values with reference to control (maximal activity, no inhibitor) from assay trials performed at least five times at 10 μg ABP concentration and 200 μM for all the other inhibitors.

order, more potent ARTase inhibitors were polymyxin B > vancomycin > cloxacillin > penicillin G and bacitracin while the rest exhibited either low to moderate action or even stimulatory effects (Table 1, Figs. 2E and F). On NADse activity, polymyxin B > cephradine and cefotaxime > bacitracin > cyclosporin A > penicillin G proved most inhibitory. To illustrate the magnitude of prevention, polymyxin B posed 21% more ARTase inhibition compared to nystatin's −18% at 0% control value without inhibitor. In addition, polymyxin concentration for half-maximal inhibition is 21-fold lower than the highest positive value for streptomycin. While vancomycin and

cloxacillin worked against ARTase and not NADse activity indicating interference on CDT–ADP-ribose^{+}–actin interaction, cephradine, and cefotaxime showed more effective NADse prevention (Table 1) (Figs. 2E and F) suggesting specific disruption of CDT–NAD interaction. Of the vitamins and derivatives tested, synthetic vitamin K_3 had strong inhibition on both activities particularly ARTase ($p < 0.01$) while thiamin showed pronounced NADse inhibition which was weaker in riboflavin and pantothenic acid (Table 1). Nicotinamide exhibited only intermediate ARTase and low NADse inhibition, reiterating action specificity to particular ADPRT.

Actin-binding proteins exhibited diverse modes of CDT inhibition

The most potent inhibitors tested were actin-binding proteins (ABPs) including myosin which was initially more potent than NAD and α-actinin which reduced ARTase activity as about efficiently as NAD. The gap in myosin potency with α-actinin at 3 μg ($p = 2.8 \times 10^{-6}$) was equalized at 12 μg concentration ($p = 0.14$) (Fig. 2H, lanes 2 and 6), suggesting the presence of α-actinin ligand in colonic lysate whose influence was dissipated at higher ABP concentration. To test our hypothesis, analytical grade muscle actin was used as substrate in photolabeling assay. α-Actinin and myosin reduced nucleotide insertion by an average of 34% and 16%, respectively, while tropomyosin posted only 4% (Fig. 2I). Indeed, there was reversal of potency suggesting endogenous factor influence which was reduced if not eliminated. On ARTase, tropomyosin was 59% and 28% less efficient than α-actinin and NAD, respectively, while troponin was not inhibitory (Fig. 2H). A hierarchy in inhibitor capacity was observed.

To further trace the mechanism of prevention, interruption of NAD hydrolysis by CDT was investigated. Parallel trend was observed whereby α-actinin showed 1.6-, 1.8-, and 14-fold higher inhibition than myosin, tropomyosin, and troponin, respectively (Table 1), establishing inability of the latter to obstruct CDT action. This suggests adduction of NAD via ABP nucleotide receptors or the presence of CDT receptor for ABP proximal to NAD binding/catalytic site or both. Sensing variation in the extent of prevention depending on CDT action, modes of ABP inhibition were assessed for functional multiplicity. With respect to NAD, kinetic analysis (Fig. 3) of α-actinin and myosin exhibited mixed-type inhibition in contrast to principally competitive action of nucleotides NAD and ATP.

Finally, in vitro observations of ABP effects on CDT-induced actin reorganization were conducted. Similar to SK1203 and ATP (200 μM/ml) exposure, confocal images of cells after 8 h treatment with CDT–α-actinin mixture showed diffuse red strands throughout the cytoplasm particularly around the submembranous cortical region (Figs. 4A and C) representing F-actin cables that totally disappeared on CDT–NAD or CDT treatment alone, manifested as cytopathic rounding with G-actin zonal green patches throughout the cell body including the nuclear region (Fig. 4B) and creation of protrusion stubs from retracting processes (Fig. 4D) due to actin disassembly and cytolysis. Difference in susceptibility was significant ($p < 0.017$) between untreated and CDT-treated cells showing 20% rounding as early as the 2nd hour and progressively thereafter up to the 8th (100% CPE). CD_{50}on the 6th hour was 71% compared to only 8% in CDT-inhibited treatment. Neutralization of CDT action by excess inhibitor/competitor was apparent in colonic cells whose basal ABP level seemed futile in counteracting CDT effects. Thus, it would be interesting to explore if contracile muscle cells would mount a more robust protection. Together, these suggest ABP preventive effects on CDTa catalysis, the exact mechanism of which awaits investigation. Further studies on the significance of ABP effects on CDT-disrupted, actin-mediated physiologic processes such as differentiation and signaling are also underway.

Discussion

We have characterized a bacterial ADPRT (CDT) whose actin-specific actions were challenged with potential inhibitors. Our preliminary studies revealed CDT

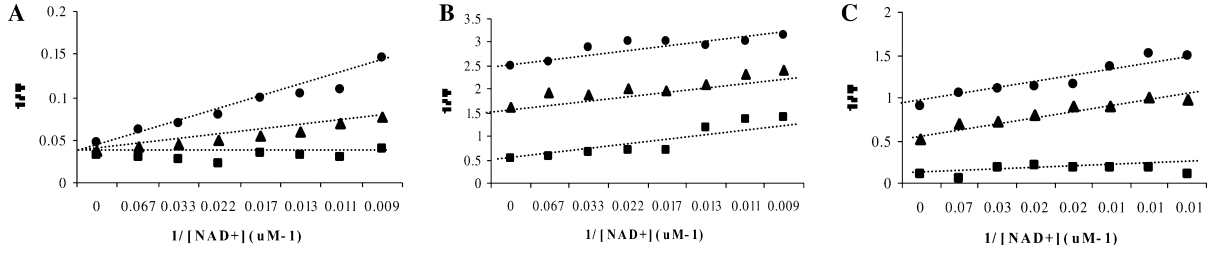

Fig. 3. Lineweaver–Burk plots of initial velocity patterns for inhibited CDT with respect to labeled NAD. At 3 μg actin, ADPRT assay was performed at indicated [^{32}P]NAD reciprocal concentrations. (A) ATP concentrations used were 50 (■), 100 (▲), and 150 (●) μM. (B) α-Actinin at 5 (■), 10 (▲), and 15 (●) μg concentrations. (C) Myosin at 5 (■), 10 (▲), and 15 (●) μg concentrations. The reciprocal of the reaction rate ($1/V$) is expressed as pixel U^{-1} h μg of muscle actin. Each data point was mean ± SD of triplicate assays.

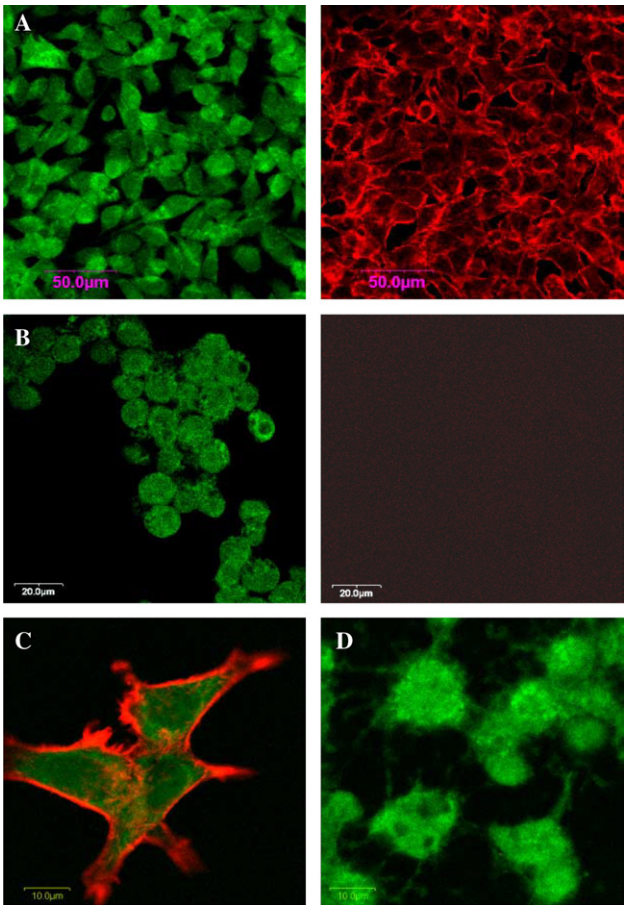

Fig. 4. Confocal images showing the effects of ATP on G- and F-actin distribution in CDT-treated HCT 116. (A) Monolayer was exposed to fresh medium (2 ml/well) containing CDTa (100 ng/ml) mixture preincubated with 15 μg α-actinin for 30 min, after 15 min CDTb (200 ng/ml) incubation. (B) Treated sequentially with CDTb and CDTa. (C–D) Magnified superimposed images of A and B, respectively. Monolayer (on coverslip) was fixed and permeabilized after 8 h treatment and stained in 500 μl PBS with 0.3 μM DNaseI-Oregon green and 0.3 μM phalloidin–TRITC for 1 h.

requirement for divalent cations for optimum catalysis, possibly through stabilization of folded nucleotide binding domain (fingers). Such roles as essential cofactor of DNA binding enzymes like in polymerases have been demonstrated [22]. Metal ions may also impose an orientating effect on CDT or actin receptors and electrostatically shield negative charges to minimize electron repulsion on attacking nucleophiles. Inhibitory effects by chelator adduction proved useful in justifying these roles with our results suggesting a rank order in metal-ion requirement for CDT functions.

In our survey of inhibitor compounds, we found that nucleotides compete for binding sites on CDT as demonstrated by ATP efficiency in NAD substitution. While nucleotide replacement in actin is possible, our data on inversely proportional reduction in radiolabeling and nucleotide concentration (Figs. 1F and G) illustrated that nucleotide substitution mainly occurred at the CDT nucleotide binding/catalytic site and demonstrated CDT affinity to NAD over other nucleotide. Besides, actin has a high affinity binding site for ATP that requires divalent cations to shift equilibrium towards monomeric (Ca^{2+}) or polymer (Mg^{2+}) state [23]. Therefore, vulnerability to nucleotide exchange may be attributed to differences in structural configuration around the NAD cavity among ADPRTs.

Although crystallographic data for CDT have not been reported, mutagenesis studies have revealed the presence of conserved amino acid residues for catalysis and NAD binding [24], that allowed classification of CDT into the cholera toxin (CT) group. They were reported to possess common motifs including β/α, Glu/Gln-X-Glu, and arom-Arg in β-strands and Ser-Thr-Ser motif at the NAD cleft [25]. Thus, CDT may follow similar mechanisms of interaction as CT which was indeed shown to have lower affinity to its cofactor compared to other ADPRTs [26]. Unlike CT, other binary A:B type toxins such as diphtheria and pertussis mediate stable docking of nicotinamide ring in the NAD cavity (β/α motif) composed of hydrophobic residues with conserved Tyr-X10-Tyr consensus whose tyrosine residues flank the nicotinamide ring creating a stable π interaction [27,28]. The lack of such three-ringed order in CT and CDT may facilitate nucleotide exchange. In terms of ARTase inhibition by nucleotides through actin, we can speculate that competition between ADP-ribose^{+} and excess nucleotide-divalent ion^{+} complex for Arg177 binding may be involved.

The antimicrobials that proved inhibitory to CDT were peptide antibiotics with modified amino acids forming motifs as in β-lactams, cyclic structures, and those linked to lipids and sugars [29]. Polymyxin B (PMB) is a cyclic cationic decapeptide that has amphipathic features. Disruption in CDT activities may have been caused by initial electrostatic interaction of its positively charged (net charge +5), arginine- and lysine-rich peptide ring residues with negatively charged interactive components of CDT or actin. This has been the primary mechanism employed in its disrupting action of bacterial membrane particularly on neutralization of the lipopolysaccharide component [30]. Since PMB is large and multicharged, it could displace stabilizing divalent cations or attach on or near essential sites blocking CDT–actin interaction.

Another cyclic peptide, bacitracin, was preventive. It binds divalent metal ions like Zn^{2+} through its His10 imidazole ring and Mn^{2+} via the thiazoline ring for its biological activity [31], making contention for metal ions seems imminent. Bacitracin has high reactivity with biomolecules like nucleotides, proteins, lipids, and receptors [32]. It is not surprising then that bacitracin is effective bacteriocide against *C. difficile*, as well as vancomycin which were both inhibitory to

CDT–ADP-ribose–actin interaction. The mechanism adopted by another cell wall active antibiotic group, the β-lactams (penicillin and cephalosporins), may involve CDT binding and steric blockage owing to structural propensity towards engagement and inactivation of transpeptidases [33]. Of the vitamins, menadione (vitamin K_3) was consistent in its strong inhibitory effects on CDT and eukaryotic poly ADPRTs [19], while nicotinamide showed moderate inhibition of CDT.

Ultimately, we found it interesting to examine if innate actin conjugants would exhibit discrepant influences on CDT activities. There are around 162 distinct ABPs known with myriad of actin-directed functions as receptor, linker, stabilizing, sequestering, and capping proteins (for review [34]). ABPs bind to overlapping receptor loci on actin surface which could interfere with CDT binding or affect catalysis. Our results suggest that sarcomeric proteins considerably reduced ARTase activity by primarily obstructing the ADP-ribosylation site of G-actin implying contact site proximity.

Based on the atomic model of actin helix [35,36], the myosin head (S1) in the rigor state binds to the peripheral face of actin subdomain 1 with a slight extension between the S1 interface and outer domain of the adjacent long-pitch monomer. These interaction sites (Fig. 5) correspond to actin residues Asp1, Glu2, Asp3, Glu4, Asp24, Asp25, Arg28, Glu93, Arg95, and Lys336 [37], and subdomain three residues Glu99, Glu100, Ala144, Ile341, Ile345, Leu349, Phe352, Pro332–333, and Trp79-Asn92 [38]. These regions overlaid by tropomyosin in the absence of Ca^{+} and S1 (tropomyosin off position) are in juxtaposition with Arg177 and may present steric impedance on ADP-ribosylation (Fig. 5). During reversible blocking (relaxed state), tropomyosin interacts with seven actin molecules along the long-pitch actin helix and, in effect, binds common acto-myosin interaction sites [36]. Comparative studies identified residues around Lys 215 and Pro307 to consist of the acto-tropomyosin interface between subdomains 3 and 4 in the on position, while Arg28, Arg95, Arg147, Cys217-Leu236, Lys238, and Lys326, 328, and 336, were present in the F-actin–tropomyosin complex [39]. These contact sites outline two distinct parallel actin regions comprising the acto-tropomyosin interface in the activated and relaxed muscle states (Fig. 5). Our results showing lower tropomyosin inhibition relative to myosin indicate that our assay conditions favor the "on" position since comparable preventive effects would have been derived in an "off" state, in which S1 and tropomyosin bind on actin coincide. In the absence of Ca^{2+}, the first troponin I inhibitory peptide (inhibit acto-myosin ATPase) interacts with actin at residues 1–7 and 19–44 anchoring troponin–tropomyosin complex on the filament [40]. Thus, acto-troponin contact sites cover a limited region of the acto-myosin interface which may explain the observed lack of inhibition by troponin (Fig. 5).

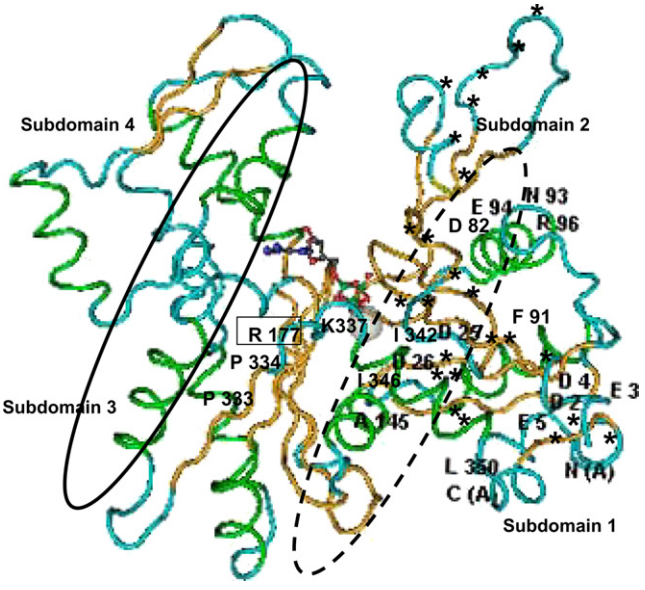

Fig. 5. Schematic illustration of G-actin showing representative interface sites with myosin (residue), tropomyosin "on" position (solid line), tropomyosin "off" position (dashed line), and troponin (asterisk). ADP-ribose acceptor residue is boxed. Contact sites with α-actinin are mainly distributed throughout subdomain 1 and are not shown for image clarity. Residues were localized based on modeling, biochemical, electron microscopic, and atomic data presented in the discussion. Structural model for 1ATN [37] was created using Cn3D4.1 program.

α-Actinin was most potent with myosin effects approaching its values in a number of trials. Through αA1–2 binding domain, its mediates lateral binding between two actin monomers at helical Trp79-Asn92 (subdomain 1and 2 interface), Ser350-Lys359 (subdomain 1 of adjacent monomer in F-actin) [41], and residues 1–12, 86–117, and 350–375 [42] that coincide with 112–125 and 360–372 identified for plastin [43]. We have traced these reactive points and found extensive occlusion around ADP-ribose acceptor and nucleotide cleft at the polymerization contact end of the molecule (Fig. 5). These could partly explain its exceptional potency as CDT inhibitor and support CDT capacity as a capping protein.

Similar reduction in glycohydrolase activity affirms partial and mixed-type inhibition by ABPs. Divergence in action and magnitude may be attributed to changes in structural form according to oxidation state, polymerization, and others. These were similarly observed in the enhanced inhibition by the micellar compared to monomeric state of arachidonic acid and in Mg^{2+} adduction by reduced α-lipoic acid [19]. Recently, the mechanism of NAD glycohydrolysis in the iota catalytic site has been proposed [44]. It involves nicotinamide release via Sn1-type cleavage of *N*-glycoside bond of the ring-like nicotinamide mononucleotide, resulting in the formation of an oxocarbenium cation intermediate stabilized by Glu380 and Ser338, followed by ADP-ribose^{+}

transfer to Arg177. These steps from NAD attachment to substrate recognition can only occur with accompanying structural dynamics which upon any molecular intervention like chelation by anion stabilizer moiety in the ABP structure can potentially disrupt the process. The precise modalities employed in abating CDT catalysis need further investigation.

In conclusion, we have quantified and compared the extent of inhibition posed by a number of molecules on various stages of ADP-ribosylation by CDT. Consistently versatile inhibitors possess reactive molecular signatures (e.g., meromyosin S1) whose application is important particularly in the design of engineered modular drug antagonists that would aid in understanding ADPRT biology and neutralize deleterious mono-ADP-ribosyltransferases.

Acknowledgment

This research work was supported by the Biomedical Research Council of Singapore under Grant No. 01/1/21/19/192.

References

[1] A. Sooki-Toth, F. Asghari, E. Kirsten, E. Kun, Cellular regulation of poly ADP-ribosylation of proteins. II. Augmentation of poly(ADP-ribose) polymerase in SV40 3T3 cells following methotrexate-induced G1/S inhibition of cell cycle progression, Exp. Cell Res. 170 (1987) 93–102.

[2] S. Obara, K. Yamada, Y. Yoshimura, M. Shimoyama, Evidence for the endogenous GTP-dependent ADP-ribosylation of the alpha-subunit of the stimulatory guanyl-nucleotide-binding protein concomitant with an increase in basal adenylyl cyclase activity in chicken spleen cell membrane, Eur. J. Biochem. 200 (1991) 75–80.

[3] J. Moss, M. Vaughan, ADP-ribosylation of guanyl nucleotide-binding regulatory proteins by bacterial toxins, Advances 61 (1988) 303–379.

[4] H. Nakajima, H. Nagaso, N. Kakui, M. Ishikawa, T. Hiranuma, S. Hoshiko, Critical role of the automodification of poly(ADP-ribose) polymerase-1 in nuclear factor-kappaB-dependent gene expression in primary cultured mouse glial cells, J. Biol. Chem. 279 (2004) 42774–42786.

[5] R. Ding, M. Smulson, Depletion of nuclear poly(ADP-ribose) polymerase by antisense RNA expression: influences on genomic stability, chromatin organization, and carcinogen cytotoxicity, Cancer Res. 54 (1994) 4627–4634.

[6] P. Gierschik, ADP-ribosylation of signal-transducing guanine nucleotide-binding proteins by pertussis toxin, Curr. Top. Microbiol. Immunol. 175 (1992) 69–96.

[7] A. Sekine, M. Fujiwara, S. Narumiya, Asparagine residue in the rho gene product is the modification site for botulinum ADP-ribosyltransferase, J. Biol. Chem. 264 (1989) 8602–8605.

[8] K.J. Pederson, A.J. Vallis, K. Aktories, D.W. Frank, J.T. Barbieri, The amino-terminal domain of *Pseudomonas aeruginosa* ExoS disrupts actin filaments via small-molecular-weight GTP-binding proteins, Mol. Microbiol. 32 (1999) 393–401.

[9] M.R. Popoff, E.J. Rubin, D.M. Gill, P. Boquet, Actin-specific ADP-ribosyltransferase produced by a *Clostridium difficile* strain, Infect. Immun. 56 (1988) 2299–2306.

[10] K. Aktories, M. Barmann, I. Ohishi, S. Tsuyama, K.H. Jakobs, E. Habermann, Botulinum C2 toxin ADP-ribosylates actin, Nature 322 (1986) 390–392.

[11] S. Perelle, M. Gibert, P. Bourlioux, G. Corthier, M.R. Popoff, Production of a complete binary toxin (actin-specific ADP-ribosyltransferase) by *Clostridium difficile* CD196, Infect. Immun. 65 (1997) 1402–1407.

[12] K. Aktories, A. Wegner, Mechanisms of the cytopathic action of actin-ADP-ribosylating toxins, Mol. Microbiol. 6 (1992) 2905–2908.

[13] J. Vandekerckhove, B. Schering, M. Barmann, K. Aktories, Botulinum C2 toxin ADP-ribosylates cytoplasmic beta/gamma-actin in arginine 177, J. Biol. Chem. 263 (1988) 696–700.

[14] C. Goncalves, D. Decre, F. Barbut, B. Burghoffer, J.C. Petit, Prevalence and characterization of a binary toxin (actin-specific ADP-ribosyltransferase) from *Clostridium difficile*, J. Clin. Microbiol. 42 (2004) 1933–1939.

[15] C.L. Hatheway, Toxigenic clostridia, Clin. Microbiol. Rev. 3 (1990) 66–98.

[16] S.P. Borriello, R.J. Carman, Association of iota-like toxin and *Clostridium spiroforme* with both spontaneous and antibiotic-associated diarrhea and colitis in rabbits, J. Clin. Microbiol. 17 (1983) 414–418.

[17] P.W. Rankin, E.L. Jacobson, R.C. Benjamin, J. Moss, M.K. Jacobson, Quantitative studies of inhibitors of ADP-ribosylation in vitro and in vivo, J. Biol. Chem. 264 (1989) 4312–4317.

[18] M. Banasik, H. Komura, M. Shimoyama, K. Ueda, Specific inhibitors of poly(ADP-ribose) synthetase and mono(ADP-ribosyl)transferase, J. Biol. Chem. 267 (1992) 1569–1575.

[19] M. Banasik, H. Komura, K. Ueda, Inhibition of poly(ADP-ribose) synthetase by unsaturated fatty acids, vitamins and vitamin-like substances, FEBS Lett. 263 (1990) 222–224.

[20] H. Barth, J.C. Preiss, F. Hofmann, K. Aktories, Characterization of the catalytic site of the ADP-ribosyltransferase *Clostridium botulinum* C2 toxin by site-directed mutagenesis, J. Biol. Chem. 273 (1998) 29506–29511.

[21] Y. Xu, V. Barbancon-Finck, J.T. Barbieri, Role of histidine 35 of the S1 subunit of pertussis toxin in the ADP-ribosylation of transducin, J. Biol. Chem. 269 (1994) 9993–9999.

[22] J.M. Berg, Y. Shi, The galvanization of biology: a growing appreciation for the roles of zinc, Science 271 (1996) 1081–1085.

[23] H.J. Kinosian, L.A. Selden, J.E. Estes, L.C. Gershman, Nucleotide binding to actin. Cation dependence of nucleotide dissociation and exchange rates, J. Biol. Chem. 268 (1993) 8683–8691.

[24] I. Gulke, G. Pfeifer, J. Liese, M. Fritz, F. Hofmann, K. Aktories, H. Barth, Characterization of the enzymatic component of the ADP-ribosyltransferase toxin CDTa from *Clostridium difficile*, Infect. Immun. 69 (2001) 6004–6011.

[25] M. Domenighini, C. Magagnoli, M. Pizza, R. Rappuoli, Common features of the NAD-binding and catalytic site of ADP-ribosylating toxins, Mol. Microbiol. 14 (1994) 41–50.

[26] T.S. Galloway, S. van Heyningen, Binding of NAD+ by cholera toxin, Biochem. J. 244 (1987) 225–230.

[27] S.F. Carroll, R.J. Collier, NAD binding site of diphtheria toxin: identification of a residue within the nicotinamide subsite by photochemical modification with NAD, Proc. Natl. Acad. Sci. USA 81 (1984) 3307–3311.

[28] C.E. Bell, D. Eisenberg, Crystal structure of diphtheria toxin bound to nicotinamide adenine dinucleotide, Biochemistry 35 (1996) 1137–1149.

[29] R.E. Hancock, D.S. Chapple, Peptide antibiotics, Antimicrob. Agents Chemother. 43 (1999) 1317–1323.

[30] Z. Oren, Y. Shai, Mode of action of linear amphipathic alpha-helical antimicrobial peptides, Biopolymers 47 (1998) 451–463.

[31] D.A. Scogin, T.O. Baldwin, R.B. Gennis, Studies on the complex formed between bacitracin A and divalent cations, Biochim. Biophys. Acta 742 (1983) 184–188.

[32] L.J. Ming, J.D. Epperson, Metal binding and structure–activity relationship of the metalloantibiotic peptide bacitracin, J. Inorg. Biochem. 91 (2002) 46–58.
[33] H.J. Rogers, C.W. Forsberg, Role of autolysins in the killing of bacteria by some bactericidal antibiotics, J. Bacteriol. 108 (1971) 1235–1243.
[34] C.G. dos Remedios, D. Chhabra, M. Kekic, I.V. Dedova, M. Tsubakihara, D.A. Berry, N.J. Nosworthy, Actin binding proteins: regulation of cytoskeletal microfilaments, Physiol. Rev. 83 (2003) 433–473.
[35] K.C. Holmes, D. Popp, W. Gebhard, W. Kabsch, Atomic model of the actin filament, Nature 347 (1990) 44–49.
[36] R.A. Milligan, M. Whittaker, D. Safer, Molecular structure of F-actin and location of surface binding sites, Nature 348 (1990) 217–221.
[37] W. Kabsch, H.G. Mannherz, D. Suck, E.F. Pai, K.C. Holmes, Atomic structure of the actin:DNase I complex, Nature 347 (1990) 37–44.
[38] R.R. Schroder, D.J. Manstein, W. Jahn, H. Holden, I. Rayment, K.C. Holmes, J.A. Spudich, Three-dimensional atomic model of F-actin decorated with *Dictyostelium* myosin S1, Nature 364 (1993) 171–174.
[39] W. Kabsch, J. Vandekerckhove, Structure and function of actin, Annu. Rev. Biophys. Biomol. Struct. 21 (1992) 49–76.
[40] R.T. McKay, B.P. Tripet, J.R. Pearlstone, L.B. Smillie, B.D. Sykes, Defining the region of troponin-I that binds to troponin-C, Biochemistry 38 (1999) 5478–5489.
[41] M.C. Lebart, C. Mejean, C. Roustan, Y. Benyamin, Further characterization of the alpha–actinin–actin interface and comparison with filamin-binding sites on actin, J. Biol. Chem. 268 (1993) 5642–5648.
[42] A. McGough, M. Way, D. DeRosier, Determination of the alpha-actinin-binding site on actin filaments by cryoelectron microscopy and image analysis, J. Cell Biol. 126 (1994) 433–443.
[43] M.C. Lebart, F. Hubert, C. Boiteau, S. Venteo, C. Roustan, Y. Benyamin, Biochemical characterization of the L-plastin–actin interaction shows a resemblance with that of alpha-actinin and allows a distinction to be made between the two actin-binding domains of the molecule, Biochemistry 43 (2004) 2428–2437.
[44] H. Tsuge, M. Nagahama, H. Nishimura, J. Hisatsune, Y. Sakaguchi, Y. Itogawa, N. Katunuma, J. Sakurai, Crystal structure and site-directed mutagenesis of enzymatic components from *Clostridium perfringens* iota-toxin, J. Mol. Biol. 325 (2003) 471–483.